INTERNATIONAL JOURNAL FOR NUMERICAL METHODS IN FLUIDS
Int. J. Numer. Meth. Fluids 2007; **53**:867–894
Published online 20 September 2006 in Wiley InterScience (www.interscience.wiley.com). DOI: 10.1002/fld.1311

Evaluation of well-balanced bore-capturing schemes for 2D wetting and drying processes

F. Marche[1,*,†], P. Bonneton[2,‡], P. Fabrie[1,§] and N. Seguin[3,¶]

[1]*Mathématiques Appliquées de Bordeaux, UMR 5466 CNRS, Université Bordeaux 1, 351 cours de la libération, 33405 Talence cedex, France*
[2]*Departement Géologie et Océanographie, UMR EPOC CNRS, Université Bordeaux 1, avenue des Facultés, 33405 Talence cedex, France*
[3]*Laboratoire Jacques-Louis Lions, Université Pierre et Marie Curie, Boite postale 187, 75252 Paris cedex 05, France*

SUMMARY

We consider numerical solutions of the two-dimensional non-linear shallow water equations with a bed slope source term. These equations are well-suited for the study of many geophysical phenomena, including coastal engineering where wetting and drying processes are commonly observed. To accurately describe the evolution of moving shorelines over strongly varying topography, we first investigate two well-balanced methods of Godunov-type, relying on the resolution of non-homogeneous Riemann problems. But even if these schemes were previously proved to be efficient in many simulations involving occurrences of dry zones, they fail to compute accurately moving shorelines. From this, we investigate a new model, called *SURF_WB*, especially designed for the simulation of wave transformations over strongly varying topography. This model relies on a recent reconstruction method for the treatment of the bed-slope source term and is able to handle strong variations of topography and to preserve the steady states at rest. In addition, the use of the recent VFRoe-ncv Riemann solver leads to a robust treatment of wetting and drying phenomena. An adapted 'second order' reconstruction generates accurate bore-capturing abilities. This scheme is validated against several analytical solutions, involving varying topography, time dependent moving shorelines and convergences toward steady states. This model should have an impact in the prediction of 2D moving shorelines over strongly irregular topography. Copyright © 2006 John Wiley & Sons, Ltd.

Received 22 September 2005; Revised 13 June 2006; Accepted 19 June 2006

KEY WORDS: non-linear shallow water; well-balanced; finite volumes; moving shoreline; topography

*Correspondence to: F. Marche, Mathématiques Appliquées de Bordeaux, UMR 5466 CNRS, Université Bordeaux 1, 351 cours de la libération, 33405 Talence cedex, France.
†E-mail: fabien.marche@math.u-bordeaux1.fr
‡E-mail: p.bonneton@epoc.u-bordeaux1.fr
§E-mail: pierre.fabrie@math.u-bordeaux1.fr
¶E-mail: seguin@ann.jussieu.fr

1. INTRODUCTION

Non-linear shallow water (NSW) equations model the dynamic of a shallow layer of homogeneous incompressible fluid and are used to describe vertically averaged flows in three-dimensional domains, in terms of horizontal velocity and depth variation. The usual conservative form of NSW equations introduced in Reference [1] is written as a first-order hyperbolic system with source terms. This set of equations is well-suited for the simulation of geophysical phenomena, such as river and oceanic flows, or even avalanches with adapted source terms. This model is also extensively used in coastal engineering, for the study of nearshore flows involving run-up and run-down on sloping beaches or coastal structures.

Wave run-up on a sloping beach is a highly complex phenomenon and computational models based on the NSW equations have been developed since a few decades, beginning with the works of Hibbert and Peregrine [2] and Kobayashi *et al*. [3]. The first difficulty which appears in the numerical simulation of run-up concerns the description of the moving shoreline. Flow properties change rapidly near the shoreline, as the water depth vanishes and the position of the shoreline is always evolving. Actually, the position of the shoreward boundary is part of the solution itself. Several methods have been proposed to track the shoreline location in the framework of finite difference methods, often only suitable for slowly varying flows, like for instance the *TRIM* model of Casulli [4], the artificial porosity method of Van't Hof *et al*. [5] or the recent works of Stelling *et al*. [6] which enable to compute rapidly varying flows as well. In a finite volume framework, various methods have also been proposed and there is essentially two approaches. The first one relies on coordinate transformations, which aim at generating a map between the time-varying physical domain and a time invariant computational domain. A Lagrangian description of the flow seems well suited for this approach and we refer to the work of Zelt [7] based on a finite elements method and to Özkan-Haller and Kirby [8] who used a spectral Fourier–Chebychev collocation. More recently, Brocchini *et al*. [9] proposed a boundary condition based on coordinate transformations and a fourth-order predictor–corrector scheme. However, these methods are not well-suited for the simulation of bore-propagation and can be difficult to use in realistic and large-scale simulations. The second approach is based on conservative schemes with fixed grids, and the direct computation of flow properties is used to predict the shoreline location. A numerical treatment of the wetting and drying processes has to be introduced and the shoreline motions can be computed with high resolution bore-capturing schemes.

The first attempt in this direction relies on Lax–Wendroff schemes [2]. Later, finite volume methods with bore-capturing abilities were developed for NSW equations. In this context, Hu *et al*. [10] proposed to use a HLL Riemann solver for the simulation of overtopping phenomenon. Recently, in References [9, 11], Brocchini *et al*. used the weight averaged flux (WAF) method introduced by Toro in Reference [12]. In the two-dimensional case, Hubbard and Dodd [13] have developed a model based on the Riemann solver of Roe. Our investigations lie in this context.

The second difficulty arising in the study of wave transformations on a sloping beach concerns the way the bed slope source term is discretized. Actually, most of the methods proposed above rely on fractional step methods (FSM). The reader is referred to Reference [14] for a description of this class of methods. Many authors such as Hu *et al*. [10] or Brocchini *et al*. [11] have applied it to take into account the varying topography in their model. This is well known today that FSM are unable to deal with strong varying topography, as they generate non-physical oscillations. The generation of errors with FSM is due to the imbalance between flux gradient and the bed slope source term. In addition, this class of method cannot preserve steady states at the discrete

DOI: 10.1002/fld

level and is clearly unable to compute the convergence towards a steady state or at least small evolutions around such states, since the splitting algorithm may introduce discretization errors which are greater than the signal itself. Therefore, numerical computation of source terms in hyperbolic systems of conservation laws has recently been improved. For the NSW equations, since the early works of Greenberg and Leroux [15] with their exact Riemann solvers on varying bottom and the quasi-steady wave propagation algorithm of Leveque [16], discretizations of the bed slope source term especially designed to preserve steady states and avoid the drawbacks of FSM have been pointed out. These methods are usually called well-balanced methods since they rely on the preservation of balancing properties for steady states. We can refer to the upwind discretization of the bed slope proposed by Vasquez-Cendon in Reference [17] and extended for two-dimensional problems in Reference [18], the surface gradient method of Zhou *et al*. [19], the flux-vector splitting scheme of Gosse [20] and more recently the VFRoe schemes of Gallouët *et al*. [21]. The application of such methods to the simulation of wave transformations on a sloping beach may be fruitful.

In this context we first propose to apply two well-balanced schemes, namely the exact well-balanced Riemann solver of Greenberg and Leroux and the well-balanced VFRoe-ncv solver, to a classical run-up problem over a sloping beach. These two solvers rely on the elegant approach which consists in directly solving Riemann problems on a non-flat bottom and have previously been validated in several test cases involving bores, steady-states preservation, multiple occurrence of dry zone and transitions between subcritical and supercritical flows over varying topography [21, 22]. From these results, these two schemes seem to be suitable for our purpose. However, we highlight their limitations and the poor results provided is the study of wave run-up, emphasizing by this way the need of better properties concerning the preservation of the water depth positivity.

Thus we introduce a new 'second order' well-balanced computational model with bore-capturing abilities and able to deal with the occurrence of dry areas. It relies on the 'hydrostatic reconstruction' introduced in Reference [23]. This method enables to take into account strong topography variations and to preserve steady states. But whereas this method was initially introduced with the use of a kinetic homogeneous solver, we choose here to use the simple VFRoe-ncv solver. The robustness and the low computational cost of this bore-capturing solver has been emphasized in Reference [21]. A symmetrizing change of variable enables this solver to properly deal with dry area, providing better properties concerning the preservation of the positivity of the water depth than the usual Roe scheme (see Reference [24]). As highlighted with extensive numerical validation against 1D and 2D analytical solutions involving moving shorelines on varying topographies, this scheme is able to accurately simulate periodic run-up and run-down phenomena and to compute with precision the preservation and the convergence towards steady states. These properties should be useful for the study of nearshore flows.

2. GOVERNING EQUATIONS AND FINITE VOLUME FORMULATION

The two-dimensional NSW equations with topography may be written as follows:

$$\mathbf{U}_{,t} + F(\mathbf{U})_{,x} + G(\mathbf{U})_{,y} = S(\mathbf{U})$$

$$\mathbf{U} = \begin{pmatrix} h \\ hu \\ hv \end{pmatrix}, \quad F(\mathbf{U}) = \begin{pmatrix} hu \\ hu^2 + \dfrac{g}{2}h^2 \\ huv \end{pmatrix}, \tag{1}$$

DOI: 10.1002/fld

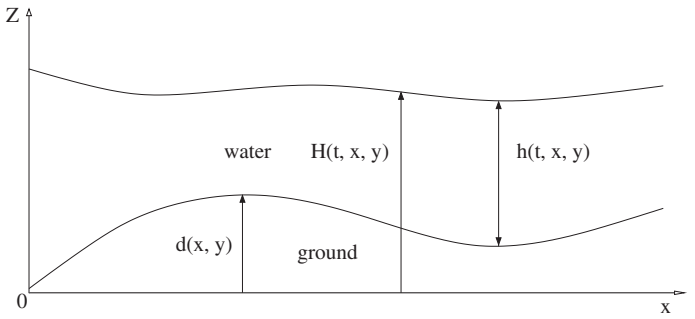

Figure 1. Surface elevation, water depth and topography.

$$G(\mathbf{U}) = \begin{pmatrix} hv \\ huv \\ hv^2 + \dfrac{g}{2}h^2 \end{pmatrix}, \quad S(\mathbf{U}) = \begin{pmatrix} 0 \\ -ghd_x \\ -ghd_y \end{pmatrix}$$

where $(\,)_{,x}$ (resp. $(\,)_{,y}$) stands for the derivate along the x direction (resp. the y direction), $\mathbf{u} = {}^t(u, v)$ is the depth-averaged velocity with u and v the scalar components in the horizontal x, y directions and h is the local water depth (see Figure 1). $\mathbf{U}$ is the vector for the conservative variables, $F(\mathbf{U})$ and $G(\mathbf{U})$ stand for the flux functions respectively along the x and y directions and $S(\mathbf{U})$ represents the bed slope source term with the bed slope $\nabla d = {}^t(d_{,x}, d_{,y})$. A two-dimensional semi-discrete finite volume formulation [25] of system (1) is given by

$$\frac{\mathrm{d}}{\mathrm{d}t}\mathbf{U}_{ij}(t) + \frac{1}{\Delta x}(\mathbf{F}^*_{i+1/2,j} - \mathbf{F}^*_{i-1/2,j}) + \frac{1}{\Delta y}(\mathbf{G}^*_{i,j+1/2} - \mathbf{G}^*_{i,j-1/2}) = \mathbf{S}_{ij} \tag{2}$$

where the cell-centred vector of conservative discrete variables is $\mathbf{U}_{ij} = {}^t(h_{i,j}, h_{i,j}u_{i,j}, h_{i,j}v_{i,j})$, $\mathbf{F}^*_{i\pm1/2,j}$ and $\mathbf{G}^*_{i,j\pm1/2}$ stands, respectively, for the numerical flux functions through the $\Gamma_{i\pm1/2,j}$ and $\Gamma_{i,j\pm1/2}$ interfaces (see Figure 2) and $\mathbf{S}_{ij}$ represents a discretization of the source term.

To define the finite volume method, we must choose a discretization method in order to compute the numerical fluxes $\mathbf{F}^*_{i\pm1/2,j}$, $\mathbf{G}^*_{i,j\pm1/2}$ and the source terms $\mathbf{S}_{ij}$.

3. WELL-BALANCED SCHEMES AND MOVING SHORELINE

The competition between the convective term and the bed-slope source term in system (1) can be highlighted when we consider that steady states are a particular kind of solutions of (1) which are independent of time. In the one-dimensional case, we obtain the following balance equation:

$$F(\mathbf{U})_{,x} = S(\mathbf{U}) \tag{3}$$

The solutions of system (3) are important since they are often obtained as limits when time tends to infinity of the solutions of system (1). Thus, the ability of a numerical scheme to accurately

DOI: 10.1002/fld

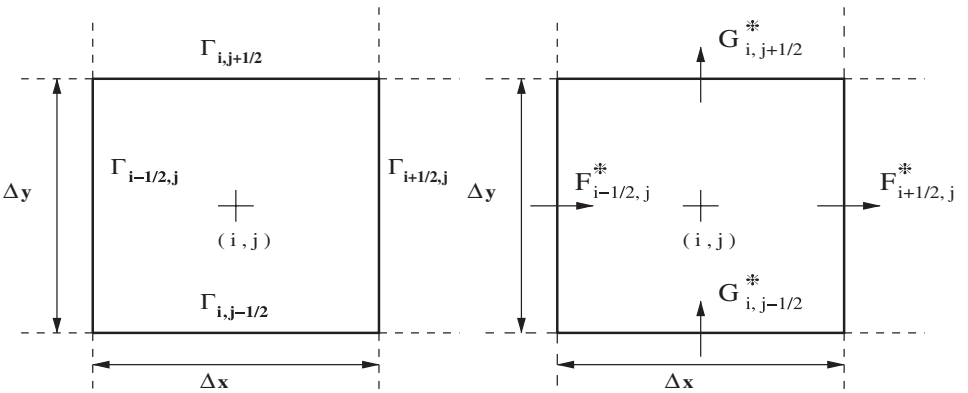

Figure 2. Discretization cell, interfaces (on the left) and numerical fluxes (on the right).

compute the convergence towards a steady state is directly linked to the way this balance property is preserved at the discrete level.

To numerically preserve this balance, several methods have been proposed, as stated above. An efficient and elegant approach is to directly solve Riemann problems with piecewise constant topography. This approach, introduced by Greenberg and Leroux [15] and extended later by Gallouët *et al*. [21] for linearized Riemann problems is the more general, since it can preserves all the steady states. We briefly recall here the formalism of these two well-balanced methods and we observe on a simple case their limitations in the prediction of moving shoreline problems.

3.1. The exact well-balanced Riemann solver

In Reference [15], Greenberg and Leroux proposed to approximate the topography with a piecewise constant function. Then, considering the topography as a new variable, an equation describing the evolution of d is added leading to a non-homogeneous Riemann problem:

$$\begin{cases} \mathbf{U}_t + F(\mathbf{U})_x = S(\mathbf{U}) \\ \mathbf{U}(x,0) = \begin{cases} (d_{\mathrm{L}}, h_{\mathrm{L}}, (hu)_{\mathrm{L}}) & \text{if } x<0 \\ (d_{\mathrm{R}}, h_{\mathrm{R}}, (hu)_{\mathrm{R}}) & \text{if } x>0 \end{cases} \end{cases} \tag{4}$$

where

$$\mathbf{U} = \begin{pmatrix} d \\ h \\ hu \end{pmatrix}, \quad F(\mathbf{U}) = \begin{pmatrix} 0 \\ hu \\ hu^2 + \dfrac{g}{2}h^2 \end{pmatrix}, \quad S_x(\mathbf{U}) = \begin{pmatrix} 0 \\ 0 \\ -ghd_{,x} \end{pmatrix}$$

The source term $-ghd_{,x}$ is reduced to a sum of Dirac masses occurring on each interface. The exact solution of the Riemann problem (4) with a bottom step is then computed. This solution is achieved by solving first the regularized Riemann problem obtained when substituting the step by a ramp. The solution for the ramp is obtained by considering all the interactions between shock waves and rarefactions arising from the left and the right side of the interface. Then, considering

DOI: 10.1002/fld

the limit in which the ramp angle increases to 90°, the solution for the step is obtained. The complete algorithm can be found in Reference [22]. This solution admits a stationary contact discontinuity located at the interface [15]. Thus, instead of computing the interface value needed to evaluate the numerical fluxes across the interface, we may compute the values at each side of the stationary contact discontinuities, denoted by $\mathbf{U}_{i+1/2}(0-, \mathbf{U}_i, \mathbf{U}_{i+1})$ and $\mathbf{U}_{i-1/2}(0+, \mathbf{U}_i, \mathbf{U}_{i+1})$ where $\mathbf{U}_{i+1/2}(x/t, \mathbf{U}_i, \mathbf{U}_{i+1})$ is the exact solution of the Riemann problem (4). The semi-discrete formulation becomes

$$\frac{\mathrm{d}}{\mathrm{d}t}\mathbf{U}_i(t) + \frac{1}{\Delta x}(F(\mathbf{U}_{i+1/2}(0-, \mathbf{U}_i, \mathbf{U}_{i+1})) - F(\mathbf{U}_{i-1/2}(0+, \mathbf{U}_i, \mathbf{U}_{i+1}))) = 0 \tag{5}$$

Note that the source term only contributes to the computation of the solution $\mathbf{U}_{i+1/2}(x/t, \mathbf{U}_i, \mathbf{U}_{i+1})$ and does not appear explicitly in (5).

The solver based on this method is robust, allowing the preservation of all steady states. Numerical benchmarks involving generations or even flooding of dry zones over varying bottom have proved the ability of the solver to deal with dry zones [22].

3.2. The well-balanced VFRoe-ncv solver

The exact well-balanced Riemann solver is more expensive than a usual Godunov method since the computation of the exact solution of problem (4) is not straightforward. To improve this, Gallouët *et al.* [21] proposed to compute exact solutions $\mathbf{U}^*_{i+1/2}(x/t, \mathbf{U}_i, \mathbf{U}_{i+1})$ of linearized Riemann problems, instead of solving directly problem (4). The second idea is to use symmetrizing non-conservative variables, leading to better properties for the preservation of the water depth's positivity in the flat case than the classical Roe or HLL solvers [24]. This class of method is called VFRoe-ncv solvers. Following Reference [21], we briefly recall the formalism of this solver:

- First, the initial Riemann problem is written under a non-conservative form, with the change of variable $\mathbf{W}(\mathbf{U}) = {}^t(d, 2c, u)$, introducing the convection matrix $C_x(\mathbf{W})$. The new Riemann problem is then linearized, averaging the convection matrix around the state $\tilde{\mathbf{W}} = (\mathbf{W}_\mathrm{L} + \mathbf{W}_\mathrm{R})/2$. It reads:

$$\begin{cases} \mathbf{W}_{,t} + C_x(\tilde{\mathbf{W}})\mathbf{W}_{,x} = 0 \\ \mathbf{W}(x, 0) = \begin{cases} \mathbf{W}_\mathrm{L} = \mathbf{W}(\mathbf{U}_\mathrm{L}) & \text{if } x<0 \\ \mathbf{W}_\mathrm{R} = \mathbf{W}(\mathbf{U}_\mathrm{R}) & \text{if } x>0 \end{cases} \end{cases} \tag{6}$$

- Then, eigenvalues and associated left and right eigenvectors of the convection matrix $C_x(\tilde{\mathbf{W}})$ are introduced, respectively noted $(\tilde{\lambda}_k)_{k=1,2,3}$, $(\tilde{\mathbf{l}}_k)_{k=1,2,3}$ and $(\tilde{\mathbf{r}}_k)_{k=1,2,3}$. The exact solution of the Riemann problem (6) is defined as follows, where $[\mathbf{W}]^\mathrm{R}_\mathrm{L} = \mathbf{W}_\mathrm{R} - \mathbf{W}_\mathrm{L}$:

$$\begin{aligned} \mathbf{W}^*\left(\left(\frac{x}{t}\right)^-, \mathbf{W}_\mathrm{L}, \mathbf{W}_\mathrm{R}\right) &= \mathbf{W}_\mathrm{L} + \sum_{\frac{x}{t}>\tilde{\lambda}_k} ({}^t\tilde{\mathbf{l}}_k \cdot [\mathbf{W}]^\mathrm{R}_\mathrm{L})\,\tilde{\mathbf{r}}_k \\ \mathbf{W}^*\left(\left(\frac{x}{t}\right)^+, \mathbf{W}_\mathrm{L}, \mathbf{W}_\mathrm{R}\right) &= \mathbf{W}_\mathrm{R} - \sum_{\frac{x}{t}<\tilde{\lambda}_k} ({}^t\tilde{\mathbf{l}}_k \cdot [\mathbf{W}]^\mathrm{R}_\mathrm{L})\tilde{\mathbf{r}}_k \end{aligned} \tag{7}$$

DOI: 10.1002/fld

- We can finally compute the solution in terms of conservative variable, using the inverse change of variable:

$$\mathbf{U}^*_{i+1/2}\left(\frac{x}{t}, \mathbf{U}_i, \mathbf{U}_{i+1}\right) = \mathbf{U}\left(\mathbf{W}^*_{i+1/2}\left(\frac{x}{t}, \mathbf{W}_i, \mathbf{W}_{i+1}\right)\right) \tag{8}$$

and compute the corresponding numerical fluxes using $\mathbf{F}^*_{i+1/2} = F(\mathbf{U}^*_{i+1/2})$.

The two values $\mathbf{W}^*((x/t)^-, \mathbf{W}_L, \mathbf{W}_R)$ and $\mathbf{W}^*((x/t)^+, \mathbf{W}_L, \mathbf{W}_R)$ are equal when $x/t \neq \tilde{\lambda}_k$. The cases $x/t = 0$ is linked to a stationary contact discontinuity, as for the exact Riemann solver, and we have therefore to compute the solution at each side of the interface. These values are then injected into the finite volume formulation (5).

This scheme is easier to implement than the exact well-balanced Riemann solver, with a far less expensive computational cost (between 10 and 100 times lower), and provides accurate results in a large number of situations. It has been validated against numerous benchmarks, involving for instance occurrences of dry zone by a double rarefaction wave over a step [21].

3.3. Numerical investigations for moving shoreline problems

From the literature, these two solvers seem to be well-suited for the study of moving shoreline problems and they have been implemented in a Godunov-like finite-volumes model. No special tracking procedure has been used for the shoreline and we have only consider a distinction between wet cells and dry cells, in which the depth of water is less than a specified threshold value $h_{\min} = 10^{-5}$. After extensive numerical validations against hydraulic benchmarks, we focus on a test for run-up phenomenon, namely the Carrier and Greenspan's periodic solution [26]. A description of this analytical solution is given in Section 5 and we only say here that this solution stands for a monochromatic wave which is let run-up and run-down on a sloping beach. Value of $\Delta x^* = 0.002$ and CFL $= 0.7$ are used (see Section 5 for details).

In Figure 3 we show the comparison between numerical results provided by the exact Riemann solver and the analytical solution for different time values during the first half period of evolution.

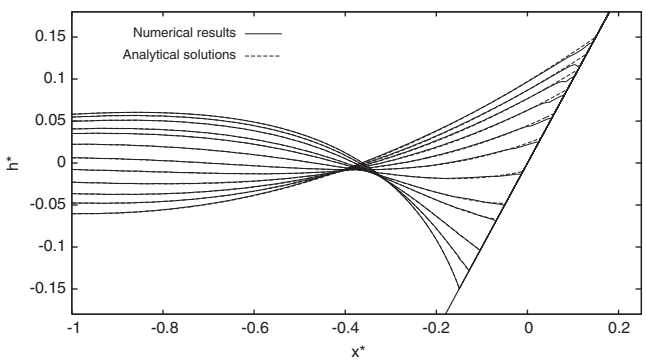

Figure 3. The Carrier and Greenspan's periodic wave solution. Comparison between numerical (solid lines) and analytical (dashed lines) results. Profiles of dimensionless water surface elevation h^* are plotted versus the onshore dimensionless coordinate x^* for the exact well-balanced Riemann solver.

DOI: 10.1002/fld

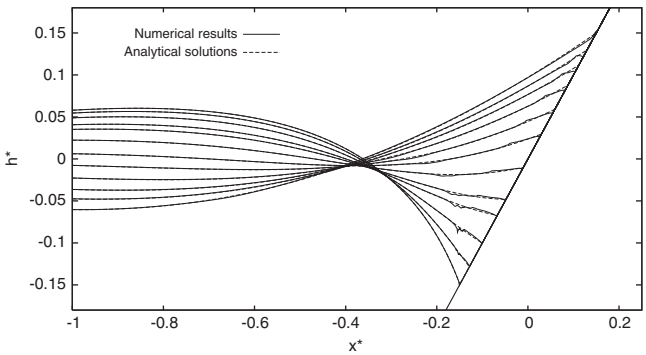

Figure 4. The Carrier and Greenspan's periodic wave solution. Comparison between numerical (solid lines) and analytical (dashed lines) results. Profiles of dimensionless water surface elevation h^* are plotted versus the onshore dimensionless coordinate x^* for the VFroe-ncv solver.

Discrepancies in the computation of the shoreline become obvious after a short time, greatly amplified during the next periods of evolution and leading to instability. Only a half period of oscillations was accurately computed with a two-times finer mesh.

Concerning the VFRoe-ncv solver, Figure 4 shows spurious oscillations propagating from the initial shoreline location and discrepancies at the shoreline also occur in the following periods. For large values of time, distortions become too important, generating instability. These non-physical oscillations may be partially justified by the fact that this scheme is not defined in the particular case of vanishing eigenvalues $\tilde{\lambda}_k$ [21].

It appears from this that even if these two schemes provide accurate simulations in many situations involving wetting and drying phenomena, they fail to compute satisfying results for this moving shoreline problems. The main reason, for both schemes, may be the lack of properties concerning the preservation of the water depth positivity near the shoreline. Actually, numerical investigations have shown that the exact Riemann solver of Greenberg and Leroux is not able to preserve such positivity in particular cases involving slowly varying topography. In the same way, if the VFRoe-ncv solver on flat bottom provides interesting properties concerning the preservation of the water depth's positivity [24], it is not rigorously extended to the well-balanced version with varying topography. That is why we present in the next section a new model which provides better properties concerning the occurrence of dry areas over varying bottom, combined with a very simple formalism and a sufficiently low computational cost for practical applications, in coastal engineering for instance.

4. THE *SURF_WB* MODEL

We propose here to use the recent hydrostatic reconstruction of Audusse *et al.*, [23]. The name 'hydrostatic reconstruction' means that the reconstruction is performed from the study of nearly static flows (i.e. flows with very small Froude number). Whereas the original method was combined with a kinetic solver, we choose here to use the VFRoe-ncv solver for homogeneous system. The main reason for this choice is that this solver is able to deal with the occurrence of dry zone [24] and the properties obtained in Reference [24] provide a better theoretical support for the preservation of the water depth positivity than the linearized solver of Roe for instance, with

DOI: 10.1002/fld

similar simple implementation and low computational cost. As it is shown in the next section, the results are excellent in practice. The reconstruction method of Audusse *et al.*, is also a simple and efficient way to obtain positivity preservation properties with varying topography and to preserve steady states 'at rest'. In the sequel we describe briefly the VFRoe-ncv solver on flat bottom and the method proposed in Reference [23].

4.1. The VFRoe-ncv solver for homogeneous system

The computation of the $\mathbf{F}^*_{i\pm1/2,j}$ fluxes is developed here. As developed in Reference [24], the symmetrizing change of variables enables to prove that intermediate states (states computed at the interfaces of the mesh) provided by the VFRoe solver remains positive and that this solver can preserve the non-negativity of the water depth at least for interface values. Due to the averaging procedure, this does not mean that cell values of water height remain positive, since the scheme does not construct the projection of the approximate solution. However, it is shown in Reference [24] that close to a wall boundary, the cell value of water height remains positive when a strong rarefaction wave develops, under a suitable CFL condition. Furthermore, numerical investigations show that in practice, cell values of the water height remains positive and that the VFRoe-ncv properties lead to excellent results for moving shoreline problems, as it is highlighted in the next section. This is not true for other approximate solvers, like the Roe or the HLL solvers. The symmetrizing change of variable $\mathbf{W}(\mathbf{U}) = {}^t(2c, u, v)$ leads to the following system:

$$\mathbf{W}_{,t} + C_x(\mathbf{W})\mathbf{W}_{,x} + C_y(\mathbf{W})\mathbf{W}_{,y} = 0 \tag{9}$$

$$C_x(\mathbf{W}) = \begin{pmatrix} u & c & 0 \\ c & u & 0 \\ 0 & 0 & u \end{pmatrix} \quad \text{and} \quad C_y(\mathbf{W}) = \begin{pmatrix} v & 0 & c \\ 0 & v & 0 \\ c & 0 & v \end{pmatrix} \tag{10}$$

where $C_x(\mathbf{W})$ and $C_y(\mathbf{W})$ are the convection matrix in the x and y directions. Considering the Riemann problem in the x direction, with this choice of 0symmetrizing variables, we obtain

$$\begin{cases} \mathbf{W}_{,t} + C_x(\mathbf{W})\mathbf{W}_{,x} = 0 \\ \mathbf{W}(x,0) = \begin{cases} ((2c)_\mathrm{L}, u_\mathrm{L}, v_\mathrm{L}) & \text{if } x<0 \\ ((2c)_\mathrm{R}, u_\mathrm{R}, v_\mathrm{R}) & \text{if } x>0 \end{cases} \end{cases} \tag{11}$$

This Riemann problem is then linearized around the averaged value $\tilde{\mathbf{W}} = (\mathbf{W}_\mathrm{L} + \mathbf{W}_\mathrm{R})/2$. The eigenvalues of the linearized convection matrix $C_x(\tilde{\mathbf{W}})$ are

$$\tilde{\lambda}_1 = \tilde{u} - \tilde{c}, \quad \tilde{\lambda}_2 = \tilde{u}, \quad \tilde{\lambda}_3 = \tilde{u} + \tilde{c}$$

where $c = \sqrt{gh}$. Then, using relations (7), the exact solution of the linearized Riemann problem is given by the sign of the eigenvalues $\tilde{\lambda}_k$. Only two cases are significant:

- If $\tilde{\lambda}_1 > 0$ or $\tilde{\lambda}_3 < 0$, then the flow is super-critical and we recover a classical upwinding. The interface value is defined as follows:

$$\mathbf{W}^*_{i+1/2,j} = \begin{cases} \mathbf{W}_i & \text{if } \tilde{\lambda}_k > 0 \ \ \forall k \\ \mathbf{W}_{i+1} & \text{if } \tilde{\lambda}_k < 0 \ \ \forall k \end{cases} \tag{12}$$

DOI: 10.1002/fld

- If $\tilde{\lambda}_1 < 0$ and $\tilde{\lambda}_3 > 0$ then the flow is subcritical and we use relations (7) to obtain the interface values. We obtain

$$c^*_{i+1/2,j} = \tilde{c} - \tfrac{1}{4}(u_{i+1,j} - u_{i,j}) \tag{13}$$

and

$$u^*_{i+1/2,j} = \tilde{u} - (c_{i+1,j} - c_{i,j}) \tag{14}$$

The value of $v^*_{i+1/2,j}$ is obtained from the sign of $\tilde{\lambda}_2$:

$$v^*_{i+1/2,j} = \begin{cases} v_{i,j} & \text{if } \tilde{\lambda}_2 > 0 \\ v_{i+1,j} & \text{if } \tilde{\lambda}_2 < 0 \end{cases} \tag{15}$$

We can finally recover conservative variables, using the inverse change of variable, and compute the numerical fluxes $\mathbf{F}^*_{i+1/2,j}$. Similar expressions result for fluxes in the y direction. It raises a fast solver with bore-capturing abilities, easy to implement, and able to deal with dry zone without any clipping treatment.

4.2. The hydrostatic reconstruction

We briefly recall here how to obtain a 'second order' well-balanced scheme satisfying the preservation of steady states 'at rest', using the method proposed in Reference [23]. This method ensures that the ability of the previous VFRoe-ncv solver to deal with the occurrence of dry areas is preserved even with a non-flat bottom [23]. The method is described in the one-dimensional case, for the sake of clarity.

The first step is to built a limited linear reconstruction of the values at each side of the mesh interfaces, following the formalism of the MUSCL method of Van Leer [27]. Considering the cell i, we compute first linear reconstructions $\mathbf{U}_{i,r}$ and $\mathbf{U}_{i,l}$ respectively at $i + 1/2-$ and $i - 1/2+$, using a *minmod* limiter. Values of $H_{i,l}$ and $H_{i,r}$, where $H = h + d$, are also reconstructed, and we deduce reconstructions of the topography $d_{i,l} = H_{i,l} - h_{i,l}$ and $d_{i,r} = H_{i,r} - h_{i,r}$. It ensures that if $u_i = 0$ and $H_i = H_{i+1}$ for all i, then $u_{i,l} = u_{i,r} = 0$ and $H_{i,l} = H_{i,r} = H_i$ for all i.

In a second step, we perform the 'hydrostatic reconstruction' of the values at each side of the mesh interfaces, taking into account the variations of the bottom and the balance obtained for flows with very small Froude number, which are considered as static flows. Interface topography values $d_{i+1/2,j}$ are defined as follows:

$$d_{i+1/2} = \max(d_{i,r}, d_{i+1,l}) \tag{16}$$

Then, the reconstruction of the water height on each side of the considered interface, which must be positivity preserving, is defined as follows:

$$h_{i+1/2-} = \max(0, h_{i,r} + d_{i,r} - d_{i+1/2}), \quad h_{i+1/2+} = \max(0, h_{i+1,l} + d_{i+1,l} - d_{i+1/2}) \tag{17}$$

and we deduce from it the complete reconstructed values on each side of the interface:

$$\mathbf{U}_{i+1/2-} = \begin{pmatrix} h_{i+1/2-} \\ h_{i+1/2-} u_{i,r} \end{pmatrix}, \quad \mathbf{U}_{i+1/2+} = \begin{pmatrix} h_{i+1/2+} \\ h_{i+1/2+} u_{i+1,l} \end{pmatrix} \tag{18}$$

DOI: 10.1002/fld

These reconstructed values are then used instead of $\mathbf{U}_i$ and $\mathbf{U}_{i+1}$ to compute the interface solution with the VFRoe-ncv solver on flat bottom. The numerical flux function $\mathbf{F}^*_{i+1/2,\,j}$ is thus defined as follows:

$$\mathbf{F}^*_{i+1/2} = F(\mathbf{U}^*_{i+1/2}(0, \mathbf{U}_{i+1/2-}, \mathbf{U}_{i+1/2+})) \tag{19}$$

where $\mathbf{U}^*_{i+1/2}(0, \mathbf{U}_{i+1/2-}, \mathbf{U}_{i+1/2+})$ is the interface value computed with the VFRoe-ncv solver on flat bottom, using the new reconstructed values $\mathbf{U}_{i+1/2-}$ and $\mathbf{U}_{i+1/2+}$ at each side of the considered interface. In the mean time, the source term $\mathbf{S}_i$ is discretized and distributed to the cell interfaces, using the reconstructed values of the water height. It gives

$$\mathbf{S}_i = \mathbf{S}_{i+1/2-} + \mathbf{S}_{i-1/2+} = \begin{pmatrix} 0 \\ \dfrac{g}{2}h^2_{i+1/2-} - \dfrac{g}{2}h^2_{i,r} \end{pmatrix} + \begin{pmatrix} 0 \\ \dfrac{g}{2}h^2_{i,l} - \dfrac{g}{2}h^2_{i-1/2+} \end{pmatrix} \tag{20}$$

This choice is motivated by the balancing requirement for static flows, with vanishing velocity. A centred source term $\mathbf{S}_{c,i}$ is added to preserve consistency and well-balancing, as developed in next subsection

$$\mathbf{S}_{c,i} = \begin{pmatrix} 0 \\ g\dfrac{h_{i,l} + h_{i,r}}{2}(d_{i,l} - d_{i,r}) \end{pmatrix} \tag{21}$$

Then, we obtain the following one-dimensional semi-discrete formulation:

$$\frac{\mathrm{d}}{\mathrm{d}t}\mathbf{U}_i(t) + \frac{1}{\Delta x}(\mathbf{F}^-_{i+1/2} - \mathbf{F}^+_{i-1/2}) = \mathbf{S}_{c,i} \tag{22}$$

with left and right numerical fluxes through the mesh interfaces defined as follows:

$$\mathbf{F}^-_{i+1/2} = \mathbf{F}^*_{i+1/2} + \mathbf{S}_{i+1/2-} = F(\mathbf{U}^*_{i+1/2}(0, \mathbf{U}_{i+1/2-}, \mathbf{U}_{i+1/2+})) + \begin{pmatrix} 0 \\ \dfrac{g}{2}h^2_{i,r} - \dfrac{g}{2}h^2_{i+1/2-} \end{pmatrix} \tag{23}$$

$$\mathbf{F}^+_{i+1/2} = \mathbf{F}^*_{i+1/2} + \mathbf{S}_{i+1/2+} = F(\mathbf{U}^*_{i+1/2}(0, \mathbf{U}_{i+1/2-}, \mathbf{U}_{i+1/2+})) + \begin{pmatrix} 0 \\ \dfrac{g}{2}h^2_{i+1,l} - \dfrac{g}{2}h^2_{i+1/2+} \end{pmatrix} \tag{24}$$

The extension to the two-dimensional framework on Cartesian meshes is straightforward. It raises a very compact formulation of the flux functions, relying on the previous homogeneous VFRoe-ncv solver, taking into account the variations of topography and able to deal with the occurrence or the flooding of dry areas. As shown in the next section, this scheme is robust and provides an accurate numerical tracking of the shoreline.

This scheme is combined with a second-order Runge–Kutta scheme, namely the Heun scheme, for time discretization.

The accuracy of this reconstruction and the slope-limiting process has been validated against classical benchmarks. The rate of convergence of the 'second order' scheme is increased compared to the classical first order model and the scheme is far less diffusive.

DOI: 10.1002/fld

4.3. Well-balancing

Assuming that $H = h + d$ is constant at time t and that $u = 0$, we have $H_{i,r} = H_{i,l}$ and so:

$$h_{i+1/2-} = \max(0, H_{i,r} - d_{i+1/2}) = \max(0, H_{i,l} - d_{i+1/2}) = h_{i+1/2+} \tag{25}$$

and by construction:

$$\mathbf{U}_{i+1/2-} = \begin{pmatrix} h_{i+1/2-} \\ 0 \end{pmatrix} = \begin{pmatrix} h_{i+1/2+} \\ 0 \end{pmatrix} = \mathbf{U}_{i+1/2+} \tag{26}$$

From this, considering (23) and (24), we obtain

$$\mathbf{F}^{-}_{i+1/2} = \begin{pmatrix} 0 \\ \dfrac{g}{2} h^2_{i,r} \end{pmatrix} \quad \text{and} \quad \mathbf{F}^{+}_{i-1/2} = \begin{pmatrix} 0 \\ \dfrac{g}{2} h^2_{i,l} \end{pmatrix} \tag{27}$$

and the semi-discrete formulation (22) leads to

$$\Delta x \frac{\mathrm{d}}{\mathrm{d}t} \begin{pmatrix} h_i(t) \\ (h_i u_i)(t) \end{pmatrix} + \begin{pmatrix} 0 \\ \dfrac{g}{2} h^2_{i,r} \end{pmatrix} - \begin{pmatrix} 0 \\ \dfrac{g}{2} h^2_{i,l} \end{pmatrix} = \begin{pmatrix} 0 \\ g \dfrac{h_{i,l} + h_{i,r}}{2} (d_{i,l} - d_{i,r}) \end{pmatrix} \tag{28}$$

Therefore, we have

$$\Delta x \frac{\mathrm{d}}{\mathrm{d}t} (h_i u_i)(t) = g \frac{h_{i,l} + h_{i,r}}{2} (h_{i,l} - h_{i,r}) + g \frac{h_{i,l} + h_{i,r}}{2} ((H_{i,l} - h_{i,l}) - (H_{i,r} - h_{i,r})) \tag{29}$$

and

$$\Delta x \frac{\mathrm{d}}{\mathrm{d}t} (h_i u_i)(t) = g \frac{h_{i,l} + h_{i,r}}{2} (H_{i,r} - H_{i,l}) = 0 \tag{30}$$

We have proved that:

$$\frac{\mathrm{d}}{\mathrm{d}t} \mathbf{U}_i(t) = 0 \tag{31}$$

and the steady states 'at rest' are preserved within this 'second order' approach. In the two-dimensional case on a Cartesian mesh, it is obvious, from the expressions of the fluxes, that we also have $(\mathrm{d}/\mathrm{d}t)(h_i v_i)(t) = 0$ and the extension to the two-dimensional framework on Cartesian meshes is straightforward. These well-balanced properties are highlighted in Appendix A, with two classical test cases.

4.4. Boundary conditions

We use two types of boundary conditions for the test cases presented in the following. The first is a *transmissive boundary condition*. Boundary cells are overwritten with the solution values in the cells of the computational domain along the boundary. It leads to a simple absorbing boundary condition, efficient for outflows configurations.

The second type is an *absorbing/generating inlet boundary condition*. We impose the values of water depth at the inlet boundary cell, to force the motion. Then characteristic curves and

DOI: 10.1002/fld

Riemann invariants are used to compute the corresponding values of the velocity, in a subcritical flow configuration. To allow the possible reflected waves to exit the domain without reflection, we use the method proposed by Kobayashi *et al.* [28]. This method has been implemented relying on the one-dimensional characteristic curves and therefore we only consider waves of normal incidence with respect to the mesh orientation.

4.5. Numerical treatment for the shoreline

We emphasize that no special 'clipping' treatment is used (i.e. we do not artificially set to zero non-physical negative values of the water depth). Moreover, no special tracking method is used to compute the location of the shoreline and we only use the direct computation of flow properties, introducing a distinction between wet and dry cells (cell drying procedure). In dry cells, the water depth h is less than a specified threshold value $h_{\min}$, which can be a very small number. For such cells, the water depth is forced to be $h_{\min}$, in order to avoid any division by zero, and the velocity is set to zero. Then, we compute the shoreline by solving Riemann problems at the interfaces between wet and dry cells, which generates no further difficulties. During the computation of the new flow properties, no special procedures are implemented to deal with the three possible configurations (wet/wet, wet/dry and dry/dry), thanks to the robustness of the VFRoe-ncv solver. The key point is that cell values issued from the hydrostatic reconstruction are given to the Riemann solver as stated above. Therefore the cell drying procedure is performed from these reconstructed values and not from the 'natural' cell values, giving excellent results in practice. The shoreline is then constructed from the mesh interfaces between wet and dry cells, without any interpolation or extrapolation as in Reference [29] for instance. In practice, we have defined $h_{\min} = 10^{-20}$ m. This value has been used in the cases presented in the next section.

4.6. Numerical stability

Explicit schemes require a careful selection of the time step to fulfil stability requirements. Classically, the time step needs to be restricted in such a way that no interaction is possible between waves from different cells during each time step. Courant, Friedrichs and Lewy defined a stability criterion for fully explicit schemes given by CFL<1 where CFL is known as the Courant number. Various definitions of this number have been proposed, leading to different time step restrictions. We choose here to define the time step as follows:

$$\Delta t \leqslant \mathrm{CFL}\, \frac{\min(\Delta x, \Delta y)}{\max_{i,j}(|U_{i,j}| + c_{i,j})} \tag{32}$$

where $c = \sqrt{gh}$. The maximum is evaluated over all the possible values of (i, j) in the computational domain.

5. NUMERICAL VALIDATION FOR WETTING AND DRYING PROCEDURE

The *SURF_WB* model has been extensively validated against numerous hydraulic cases but in this section we focus on moving shoreline problems in the one and two-dimensional framework. In the one-dimensional case, we perform comparisons with analytical solutions for waves propagating over a uniform sloping beach with run-up, run-down and eventually reflexion. In the two-dimensional

DOI: 10.1002/fld

case, we validate the model against analytical solutions for periodic oscillating motions with moving boundaries in a parabolic basin. The 'second order' scheme is used for all the cases presented here. The grids are uniform, with $\Delta x = \Delta y$ in the two-dimensional case.

5.1. 1D assessments

5.1.1. The Carrier and Greenspan transient solution. As a first validation of the shoreline description, the initial water surface elevation is assumed to be depressed near the shoreline, the fluid held motionless and then released at $t = 0$. This initial condition is the lower curve in Figure 5. Let l be the typical length scale of this specific problem and α the beach slope. Non-dimensional variables are defined as follows:

$$x^* = x/l, \quad \xi^* = \xi/(\alpha l), \quad u^* = u/\sqrt{g\alpha l}, \quad t^* = t/\sqrt{l/\alpha g}, \quad c^* = \sqrt{(\xi^* - x^*)} \tag{33}$$

Carrier and Greenspan [26] used a hodograph transformation to solve the NSW equations and obtain an analytical solution, relying on the introduction of the two dimensionless variables σ^* and λ^*, respectively, linked to the space and time coordinate. These variables are defined as follows:

$$\sigma^* = 4c^*, \quad \lambda^* = 2(u^* + c^*) \tag{34}$$

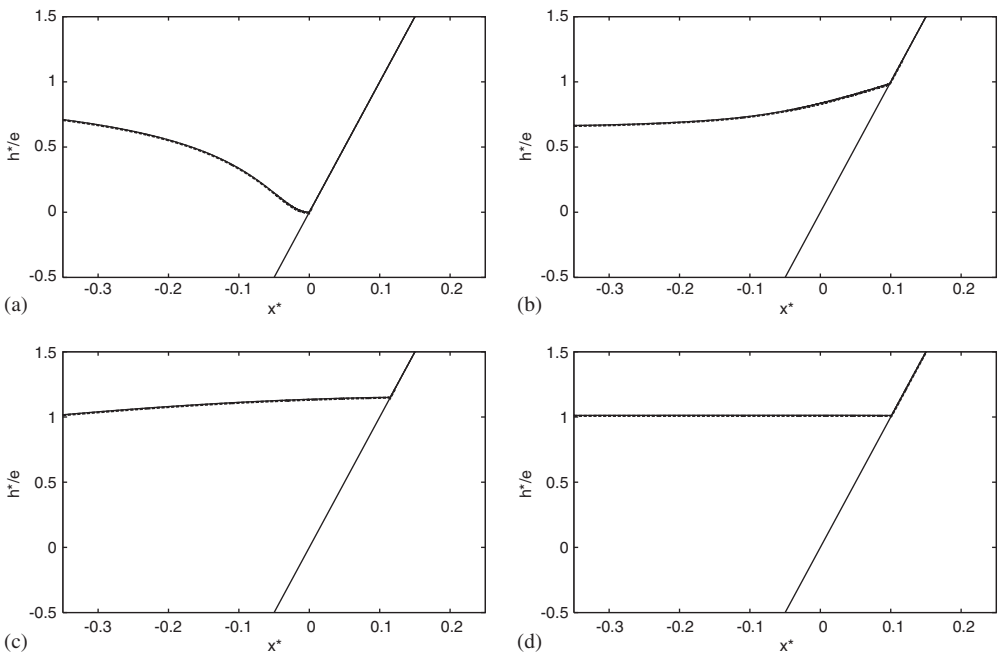

Figure 5. The Carrier and Greenspan's transient solution. Comparison between numerical results (in solid lines) and analytical solutions (in dotted lines) for the surface elevation. Profiles of water depth h^*/e are plotted versus the onshore coordinate x^*, for: (a) $t^* = 0$ s; (b) $t^* = 1$; (c) $t^* = 2$; and (d) $t^* = 10$.

DOI: 10.1002/fld

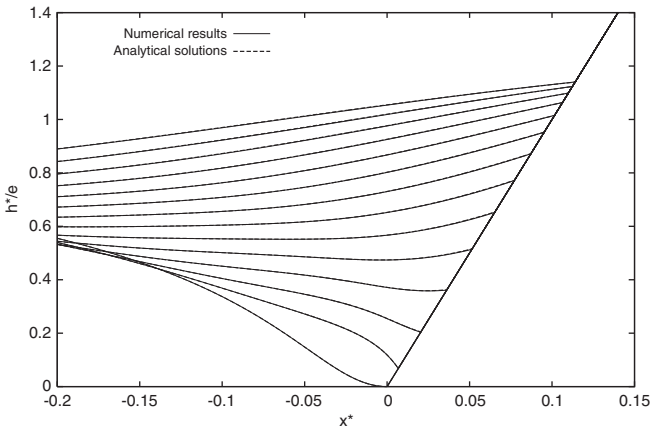

Figure 6. The Carrier and Greenspan's transient solution. Comparison between numerical results (in solid lines) and analytical solutions (in dotted lines) for the surface elevation. Zoomed profiles of water depth h^*/e are plotted versus the onshore coordinate x^*, for different values of time t^*, increasing from $t^*=0$ (bottom curves) to $t^*=1.4$ (top curves).

Starting from the one-parameter family of wave-forms at $t=0$:

$$\begin{cases} \xi^* = e\left[1-\dfrac{5}{2}\dfrac{a^3}{(a^2+\sigma^{*2})^{3/2}}+\dfrac{3}{2}\dfrac{a^5}{(a^2+\sigma^{*2})^{5/2}}\right] \\ x^* = -\dfrac{\sigma^{*2}}{16}+e\left[1-\dfrac{5}{2}\dfrac{a^3}{(a^2+\sigma^{*2})^{3/2}}+\dfrac{3}{2}\dfrac{a^5}{(a^2+\sigma^{*2})^{5/2}}\right] \end{cases} \tag{35}$$

where $a=\frac{3}{2}(1+0.9e)^{1/2}$ and e is a small parameter which characterizes the surface elevation profile, Carrier and Greenspan [26] have obtained the analytical solution, using some relations between dimensionless ordinary variables, hodograph coordinates and a potential function depending on this specific problem. This set of equations is solved by iterative processes and we use the values of this analytical solution at the left boundary as the inlet left boundary condition in order to generate the motion.

During the evolution, the maximum penetration distance attained by the wave occurs when the coastline velocity is zero. The shoreline rises above the mean sea level of value e and then the water surface elevation asymptotically settles back to it. The bottom slope α is taken to be $\frac{1}{50}$, the results are presented here for $e=0.1$ and the initial surface profile (35) is imposed in the dimensional case with the length scale $l=20\,\mathrm{m}$. Values of $\Delta x^*=0.002$ and $\mathrm{CFL}=0.7$ have been used for this test. Figures 5 and 6 show comparisons between numerical results and analytical solutions for the surface elevation. These surface elevation profiles have been scaled with the parameter e. We show in Figure 5 the whole surface elevation profiles at four values of time. This highlights the accuracy of the computation for large values of t^* and during the asymptotic convergence towards the mean level. In Figure 6, zoomed surface elevation profiles near the shoreline are plotted versus the onshore coordinate. We see on both figures that the *SURF_WB* model provides excellent agreements with the analytical solution at the two level of scaling. Lastly, we show in Figure 7 the time series of the shoreline surface elevation. The shoreline position asymptotically settles to e and the model provides stability and a good accuracy in the computation of this slow

DOI: 10.1002/fld

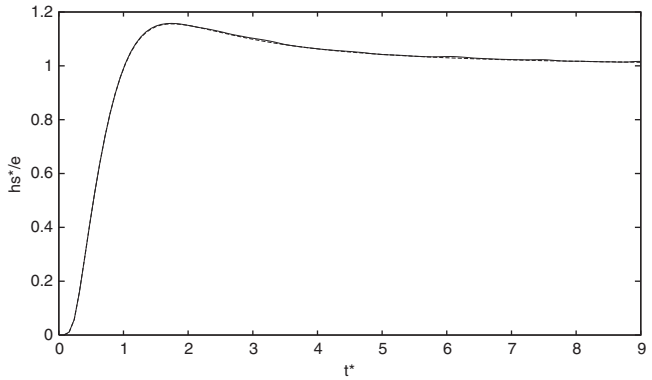

Figure 7. The Carrier and Greenspan's transient solution. Comparison between numerical results (in solid line) and the analytical solution (in dotted lines) for the motion of the shoreline. Surface elevation of the dimensionless shoreline h_s^*/e is plotted versus dimensionless time coordinate t^*.

convergence. We emphasize that the use of FSM for this test leads to instabilities for large values of time, since errors induced by the discretization may become greater than the variations of the solution. For this reason, numerical results for large values of t^* are rarely shows in the literature.

5.1.2. The Carrier and Greenspan periodic wave solution. In this test, a monochromatic wave is let run-up and run-down on a plane beach. This represents the motion of a periodic wave of dimensionless amplitude A^* and frequency ω^* travelling shoreward and being reflected out to sea, generating a standing wave. The previous dimensionless quantities (33) are used and the analytical solution is obtained using the hodograph coordinates (34). We obtain for this specific problem:

$$\begin{cases} u^* = -\dfrac{A^* J_1(\sigma^*)\sin(\lambda^*)}{\sigma^*} \\ \xi^* = \dfrac{A^*}{4} J_0(\sigma^*)\cos(\lambda^*) - \dfrac{u^{*2}}{4} \\ t^* = \dfrac{1}{2}\lambda^* - u^*;\ x^* = \xi^* - \dfrac{\sigma^{*2}}{16} \end{cases} \tag{36}$$

where J_0 and J_1 are the Bessel functions of zero and first order and the dimensionless frequency ω^* is equal to one. This analytical solution is frequently used to validate the ability of numerical models to deal with run-up and run-down phenomenon and to study the dynamic of waves near a continental shelf and we refer to Reference [26] for a complete description. This expression is only valid for $0 \leqslant A^* \leqslant 1$ and $A^*/4$ represents the maximum vertical excursion of the shoreline. The value of this solution at $t = 0$ is supplied as initial condition and the analytical variation of the surface elevation at the left boundary is used as an offshore boundary condition.

We compute this numerical solution with a dimensionless amplitude $A^* = 0.6$, a length scale $l = 20\,\text{m}$ and a bottom slope $\alpha = 1/30$. Extensive numerical investigations show that *SURF_WB* is robust enough to deal with a large range of bottom slope. The numerical results are compared to the analytical solution for a significant range of time, to ensure that small instabilities, which may eventually be amplified later, are not generated. We show in Figure 8 the comparison for the surface elevation, at different values of time t^* between $3T^*$ and $3T^* + T^*/2$, where T^* is

DOI: 10.1002/fld

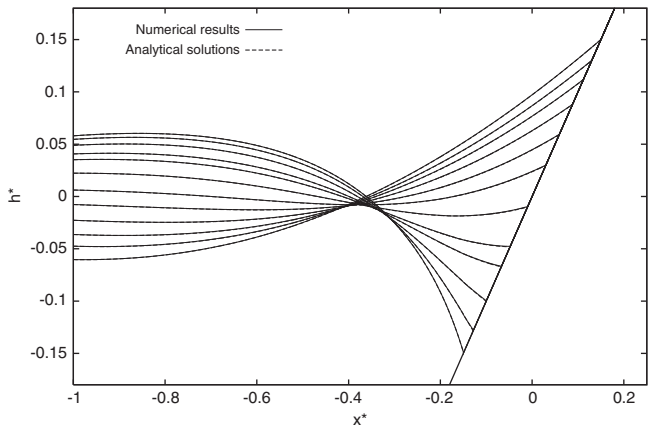

Figure 8. The Carrier and Greenspan's periodic wave solution. Comparison between numerical results (solid lines) and analytical solutions (dotted lines) for the surface elevation. Profiles of water surface elevation h^* are plotted versus the onshore coordinate x^* for different values of time t^* increasing from $t^* = 3T^*$ to $t^* = 3T^* + T^*/2$.

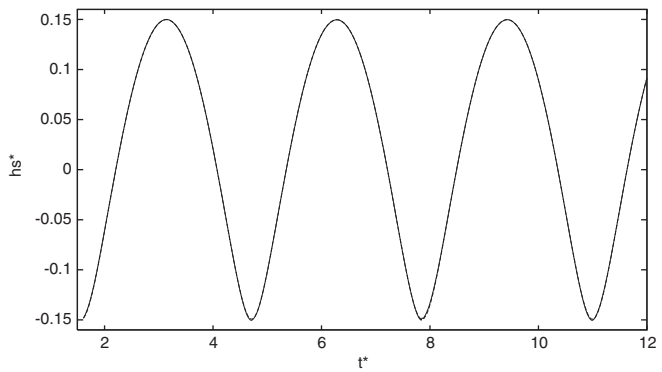

Figure 9. The Carrier and Greenspan periodic wave solution. Comparison between numerical results and the analytical solution for the vertical motion of the shoreline. Water surface elevation of the shoreline h_s^* is plotted versus the dimensionless time coordinate t^*, during three periods.

the dimensionless period of the oscillations. Value of $\Delta x^* = 0.002$ and $\mathrm{CFL} = 0.7$ are used. We observe that the moving shoreline is accurately computed even after a few periods. We can observe in Figure 9 time series of the surface elevation at the shoreline. The accuracy of the results is obvious and a comparison with results found in the literature (see Reference [9] for instance), highlights the quality of these results. In addition, it is worth mentioning that the L^2 error is not amplified and never goes over three per cent during ten periods. We can see in Figure 10 the L^2-convergence curves for the water height and the velocity. The used L_2-error is defined at the nth time for h and $\mathbf{u}$ as follows:

$$\mathrm{Err}^{L_2}(h) = \left\{ \frac{\sum_{i,j} (h_{ij}^n - h_a)^2}{\sum_{i,j} h_a^2} \right\}^{1/2} \tag{37}$$

DOI: 10.1002/fld

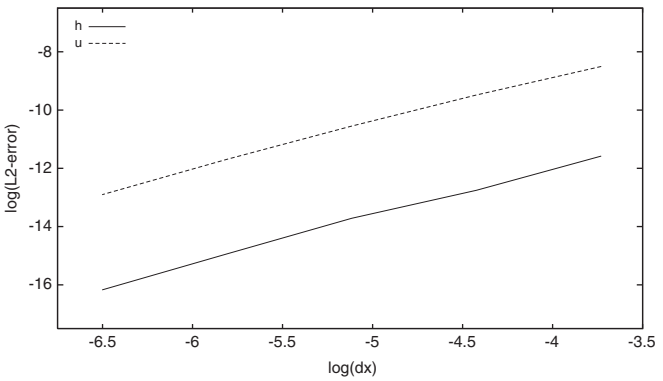

Figure 10. The Carrier and Greenspan's periodic solution. L^2-convergence curves for the surface elevation h^* (in solid line) and the velocity u^* (in dashed–dots line) at $t^* = 1.5$. $\log(L^2\text{-error})$ is plotted versus $\log(\Delta x)$ at $t^* = 1.5$.

$$\mathrm{Err}^{L_2}(\mathbf{u}) = \left\{ \frac{\sum_{i,j} [(u_{ij}^n - u_a)^2 + (v_{ij}^n - v_a)^2]}{\sum_{i,j} [u_a^2 + v_a^2]} \right\}^{1/2} \tag{38}$$

where $U_a = {}^t(h_a, (hu)_a, (hv)_a)$ represents the analytical solution at the appropriate time. This error measure takes into account the numerical errors in the computation of the surface elevation and the velocity for all computational points at a given time. The measured rate of convergence are above 1.66 for the water height and 1.63 for the velocity.

5.1.3. The Synolakis run-up solution. Solitary wave run-up phenomenon were investigated experimentally and numerically by Synolakis [30]. Although it is well known that solitary waves are not classical solutions of the NSW equations, it has been found that for small amplitudes and over limited distances, the Synolakis solution provides a good model of beach inundation and reflection by a solitary wave. This solution has been extensively used in order to validate experimental and numerical models.

In this test, a solitary wave travelling from the shoreward is let run-up and run-down on a plane beach, before being fully reflected and evacuated from the computational domain. The topography for this test of wave run-up and reflection is made of a constant depth area juxtaposed with a plane sloping beach of slope β.

The initial condition is a solitary wave, centred at a distance x_1 from the toe of the beach equal to its half wave length:

$$\begin{aligned} h(x, t=0) &= \frac{H}{D} \operatorname{sech}^2(\gamma(x - x_1)) \\ u(x, t=0) &= \sqrt{\frac{g}{D}} \cdot h_0(x) \end{aligned} \tag{39}$$

DOI: 10.1002/fld

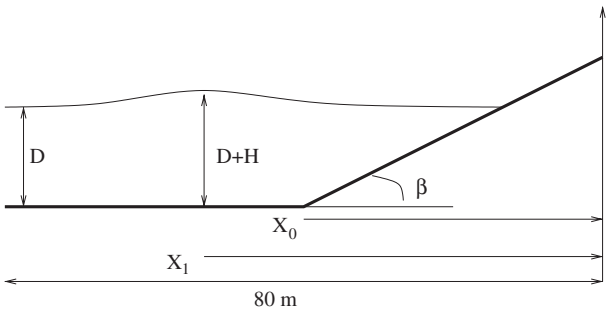

Figure 11. Definition sketch for the initial condition of the Synolakis' solution.

where

$$\gamma = \sqrt{\frac{3H}{4D}} \quad \text{and} \quad x_1 = \sqrt{\frac{4D}{3H}}\,\text{arcosh}\left(\sqrt{\frac{1}{0.05}}\right) \tag{40}$$

is the initial position of the centre of the solitary wave (see Figure 11). The initial amplitude is set to be $H = 0.019$ m, the mean water depth is $D = 1.0$ m and the beach slope is defined with $\cot(\beta) = 19.85$. The analytical solution, obtained by the combination of the Carrier and Greenspan's hodograph transformation and a Fourier transform is provided in the original paper of Synolakis [30]. A simplified form is exposed in Reference [10]. For this test, we have used $\Delta x = 0.02$ and the CFL is set to 0.8. The numerical results are compared with the analytic solution in Figure 12 for different values of time between the initial condition and the complete evacuation of the wave from the computational domain. No discrepancies are observable. Time series of the evolution of water height at $x = 72.5$ m are presented in Figure 13. We emphasize that after the total reflection of the incident wave, the convergence towards the steady state at rest is accurately computed whereas FSM are simply unable to provide any valuable results since non-physical oscillations are generated. In the literature, such results showing the computation of this steady states using bore-capturing finite-volumes methods are not shown.

5.2. 2D assessments

Few analytical solutions are available for the two-dimensional NSW equations with free moving boundary. In his study, Thacker [31] provides two different classes of solutions corresponding to time-dependent non-linear oscillations in parabolic basins. The motion is oscillatory with a small enough amplitude, imposed by the long wave assumption, and there is no energy dissipation. For these two tests, the flow takes place inside a parabola of revolution defined as

$$d(r) = -h_0\left(1 - \frac{r^2}{a^2}\right) \tag{41}$$

on the computational domain $[-2, 2] \times [-2, 2]$, where h_0 is the depth of water at the centre point for a zero elevation and a is the distance from the centre point to the zero elevation of the shoreline (see Figure 14). For the two following tests, we use $\Delta x = \Delta y = 0.008$ m and the CFL is set to 0.6.

DOI: 10.1002/fld

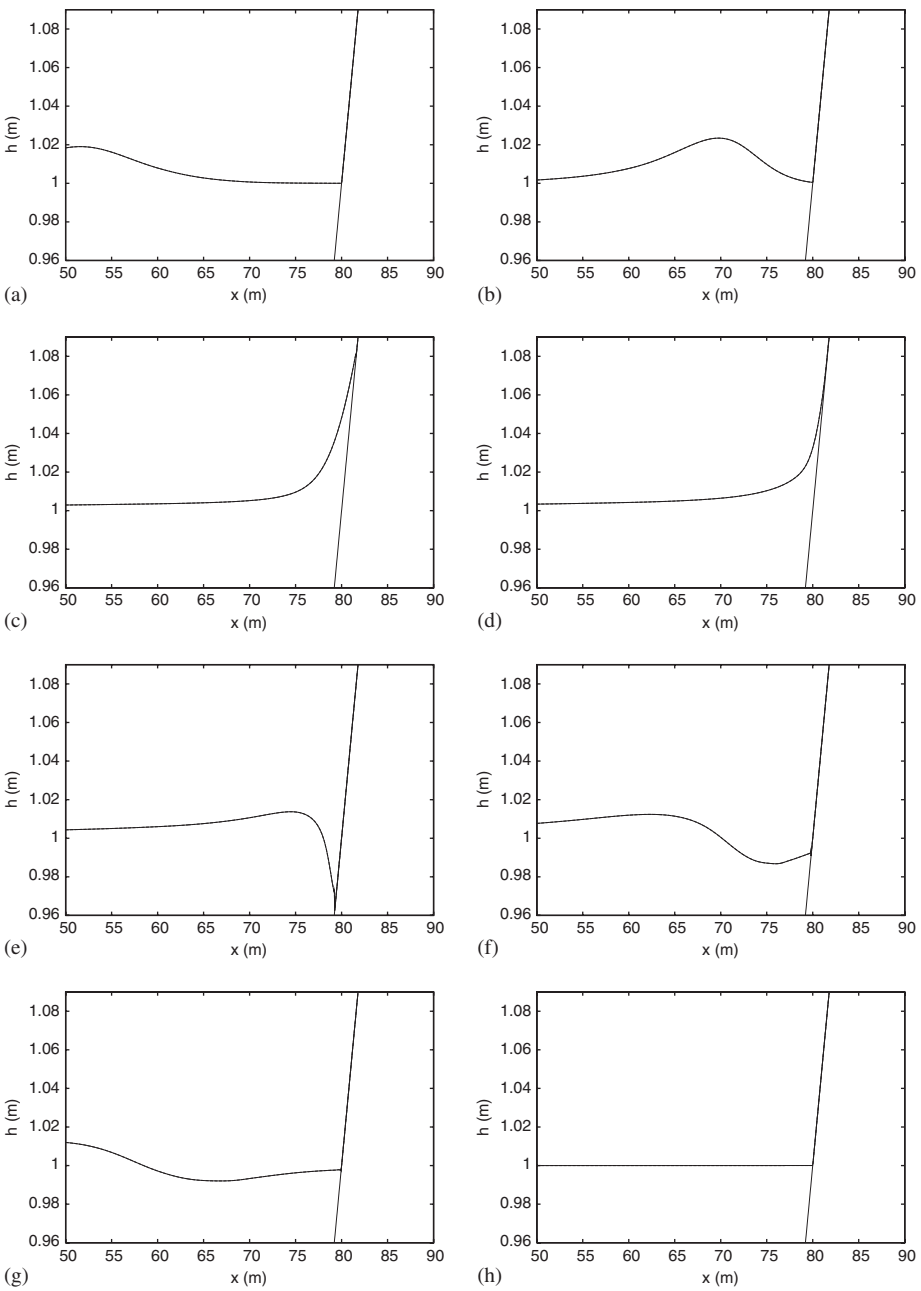

Figure 12. The Synolakis run-up solution. Comparison between numerical results (solid lines) and analytical solution (dotted lines) for the surface elevation. Profiles of water depth h are plotted versus the onshore coordinate x for: (a) $t = 3.0$ s; (b) $t = 9.0$ s; (c) $t = 17.0$ s; (d) $t = 19.5$ s; (e) $t = 23.0$ s; (f) $t = 28.0$ s; (g) $t = 32.5$ s; and (h) $t = 75.0$ s.

DOI: 10.1002/fld

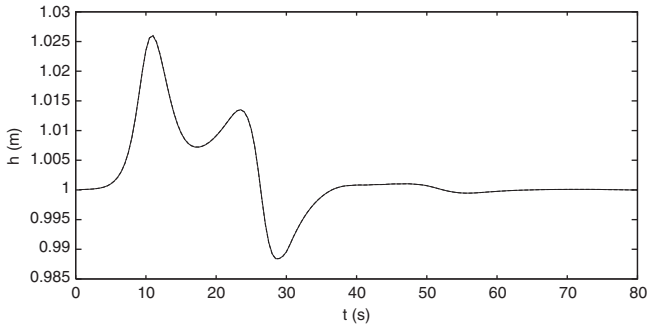

Figure 13. The Synolakis run-up solution. Time series of the water height: comparison between numerical results (solid line) and analytical solution (dotted line). The profile of the water height h is plotted versus the time coordinate t at $x = 72.5$ m.

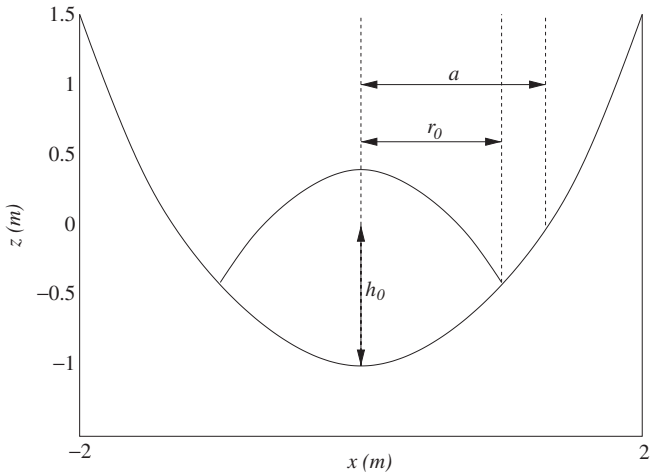

Figure 14. Centreline shape of the basin and initial free surface for the Thacker's curved solution.

5.2.1. Thacker's curved solution. The curved solution provides in Reference [31] is given by

$$h(r,t) = h_0\left[\frac{(1-A^2)^{1/2}}{1-A\cos(\omega t)} - 1 - \frac{r^2}{a^2}\left(\frac{1-A^2}{(1-A\cos(\omega t))^2} - 1\right)\right]$$
$$u = \frac{1}{1-A\cos(\omega t)}\left(\frac{1}{2}\omega x A\sin(\omega t)\right), \quad v = \frac{1}{1-A\cos(\omega t)}\left(\frac{1}{2}\omega y A\sin(\omega t)\right) \tag{42}$$

where the frequency ω is given by $\omega = \sqrt{8gh_0/a^2}$, r is the distance from the centre point, r_0 the distance from the centre point to the point where the shoreline is initially located (see Figure 14) and $A = (a^2 - r_0^2)/(a^2 + r_0^2)$.

DOI: 10.1002/fld

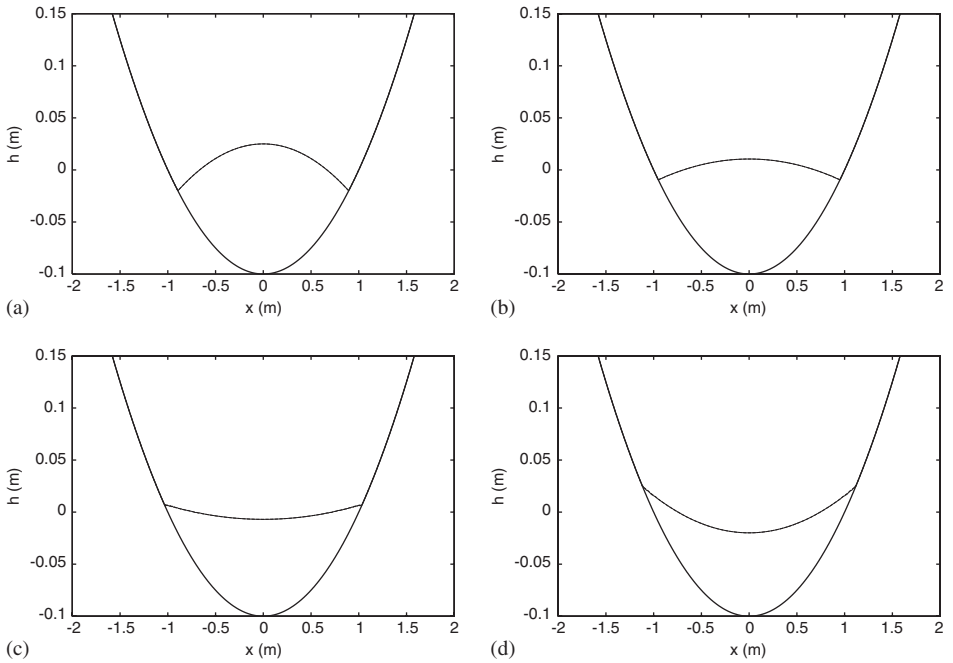

Figure 15. Thacker's curved solution. Comparison between numerical results (in solid lines) and analytical solution (in dotted lines) for the centreline free surface profile. Water surface elevation profiles h are plotted versus the x coordinate, for $y=0$, for: (a) $t=3T$; (b) $t=3T+T/6$; (c) $t=3T+T/3$; and (d) $t=3T+T/2$, where T is the oscillations period.

The analytical solution at $t=0$ is supplied as initial condition. The depth profile for the basin and the definition of a, r_0 and h_0 are shown in Figure 14. The values used for this numerical test are $a=1$, $r_0=0.8$ m and $h_0=0.1$ m. The centreline initial condition (for $y=0$) is shown in Figure 15(a) together with comparisons between numerical and analytical results at three different times. The surface elevation profiles are computed after three periods T and are in excellent agreement with the analytical solution. Furthermore, it seems that no spurious oscillations are present near the shoreline even after three periods.

In Figure 16, we focus on the run-up and run-down phenomena during a half period. We see on this zoom that actually, very small distortions appear in the intermediates states between the minimum and maximum surface elevation. But these distortions are small enough to be smoothed during the next numerical iterations and thus, they do not propagate. These results are very satisfying when compared to those introduced in Lynett *et al*. [29], where a complex extrapolation method is used, combined with smoothing procedures to avoid non-physical instabilities.

We show in Figure 17 the L^2-convergence curves for the water height h and the velocity $\mathbf{u}$. The rate of convergence is around 1.4 for the water height and 1.2 for the velocity.

5.2.2. Thacker's planar solution. This test case is perhaps the most difficult for the numerical model since it involves a wetting and drying procedure on a no radially symmetric configuration.

DOI: 10.1002/fld

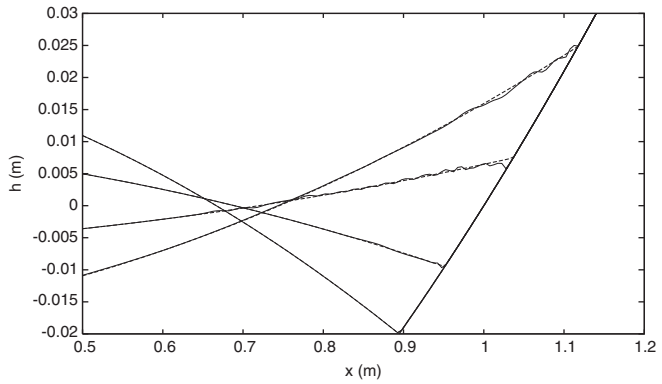

Figure 16. Thacker's curved solution. Zoomed centreline free surface profiles for the surface elevation, near the shoreline. Analytical and numerical profiles are plotted versus the x coordinate, for $y = 0$ for different $t = 3T$, $t = 3T + T/6$, $t = 3T + T/3$, $t = 3T + T/2$.

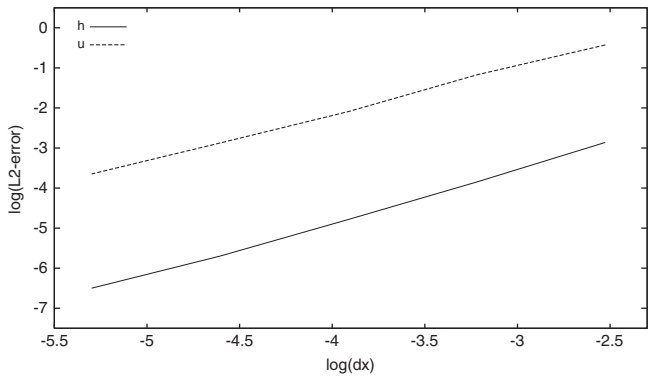

Figure 17. Thacker's curved solution. L^2-convergence curves for the surface elevation h (in solid line) and the velocity $\mathbf{u}$ (in dashed–dots line). $\log(L^2\text{-error})$ is plotted versus $\log(\Delta x)$ at $t = 3\,\text{s}$.

The exact periodic solution provided in Reference [31] is given by

$$h(x, y, t) = \frac{\eta h_0}{a^2}(2x\cos(\omega t) + 2y\sin(\omega t) - \eta)$$
$$u = -\eta\omega\sin(\omega t), \quad v = \eta\omega\cos(\omega t) \tag{43}$$

where $\omega = \sqrt{2gh_0}/a$. The values used for this numerical test are $a = 1$, $\eta = 0.5\,\text{m}$ and $h_0 = 0.1\,\text{m}$. This solution evaluated at $t = 0$ is used as an initial condition. The moving shoreline is a circle in the (x, y) plane and the motion is such that the centre of the circle orbits the centre of the basin, while the surface remains planar with constant gradient at any given instant. Numerical results are compared to the analytical solution in Figure 18. We observe an accurate matching even after two periods. We note a small distortion near the shoreline, which can be reduced with a finer mesh. The moving shoreline is accurately computed during several periods with no signs

DOI: 10.1002/fld

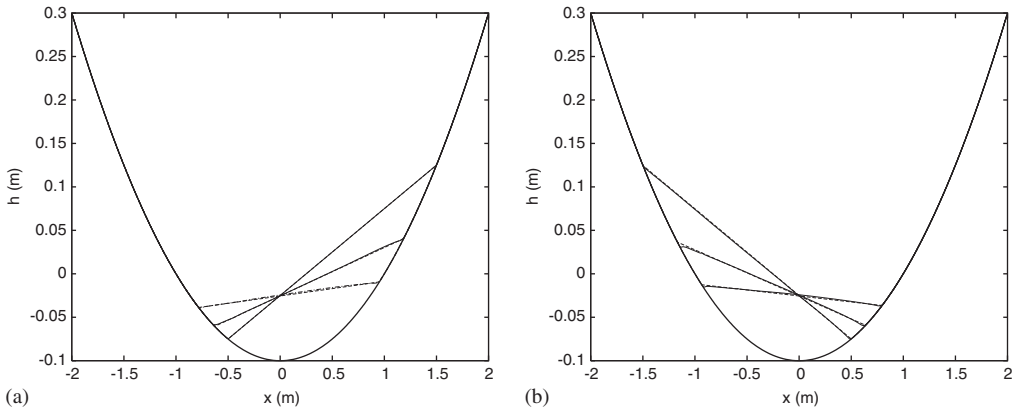

Figure 18. Thacker's planar solution. Comparison between numerical results (in solid lines) and analytical solution (in dotted lines). Centreline free surface profiles for the surface elevation h are plotted versus the x coordinate, for $y = 0$, at: (a) $t = 2T$, $t = 2T + T/6T$, $t = 2T + T/5T$; and (b) $t = 2T + T/4$, $t = 2T + T/3$, $t = 2T + T/2$.

of amplified spurious oscillations. Once again, these results are very satisfying when compared to those obtained by Hubbard and Dodd [13], using an adaptive mesh refinement algorithm.

6. CONCLUSION

We introduce in this paper a new two-dimensional NSW model, named *SURF_WB*, for predicting wetting and drying processes on varying topographies. This model relies on the combination of the VFRoe-ncv Riemann solver for homogeneous systems, which is able to deal with the occurrence of dry areas, and the recent hydrostatic reconstruction which provides a well-balanced treatment of the bed slope source term. In addition, a MUSCL reconstruction is performed to achieve a 'second order' accuracy. It raises a fast and accurate bore-capturing well-balanced method, easy to implement and able to preserve steady states at rest. This model has been validated against analytical solutions in situations involving multiple moving shorelines, strong variations of bed slope and convergence towards a steady state. This scheme introduces very little artificial viscosity and numerical results are in very good agreement with analytical solutions. Furthermore, we have shown that the application of well-balanced schemes for this class of problems is not trivial, since two others schemes, which have been extensively validated in situations involving occurrence of dry area and strong bottom variations, have failed to provide accurate results in moving shoreline problems. From these investigations, the *SURF_WB* model appears as an efficient tool which can be of a great utility for simulations of wave's run-up and run-down, especially in coastal engineering. A qualitative comparison with models introduced in the literature shows that *SURF_WB* results are at least as accurate as those presented by Brocchini *et al.* [9] with their fixed grid method and sometimes even with their complex coordinates transformation method. Concerning the two-dimensional cases, the results introduced here are almost as accurate as results obtained in the literature with extrapolation methods and adaptive mesh refinement algorithms. In addition *SURF_WB* enables us to overcome the problems due to the fractional step method which

DOI: 10.1002/fld

is used in these models. From these assessments, it can also be noticed that *SURF_WB* is able to deal with strong variations of topography as well as the robust and accurate exact well-balanced Riemann solver of Leroux *et al*., and ensures more accurate results for moving shoreline problems.

In recent studies [32] we investigate the use of this model for the simulation of two-dimensional run-up in coastal areas and the study of wave-induced mean currents and macro-vorticity in the surf and swash zone, over realistic topographies. As it has been emphasized in Reference [33], spurious vorticity may be generated by the imbalance between flux gradient and source term of their model. The use of *SURF_WB* helps to overcome these drawbacks.

APPENDIX A

This section is devoted to the numerical validation of the *SURF_WB* model against several classical test cases.

A.1. Transcritical flow over a bump

We present here a classical test of a constant discharge transcritical flow without shock over a bump and we refer to Reference [34] for a complete description of this test. The main interest is to study the convergence towards a steady state and the improvement obtained within the well-balanced approach. The topography is defined as in Reference [21]. The test is performed with 200 cells and the CFL number is set to 0.4. The boundary conditions are a positive imposed discharge $Q_{\text{in}} = 1.53\,\text{m}^2/\text{s}$ on the left boundary, and a imposed height $h_{\text{out}} = 0.66\,\text{m}$ on the right boundary. The initial condition is set to $h_0 = h_{\text{out}}$ and $Q = 0$. The analytical solution for the surface elevation is smooth with a decreasing part, including a sonic point. The solution at the right of this sonic point is supercritical and the boundary condition h_{out} is only used when the flow is subcritical, during the transient part of the simulation. The results are plotted at $t = 200\,\text{s}$. We can observe in Figure A1(a) that, as we are far from a steady state 'at rest', the results for the surface elevation provided by *SURF_WB* and the FSM (also based on the VFRoe-ncv solver for

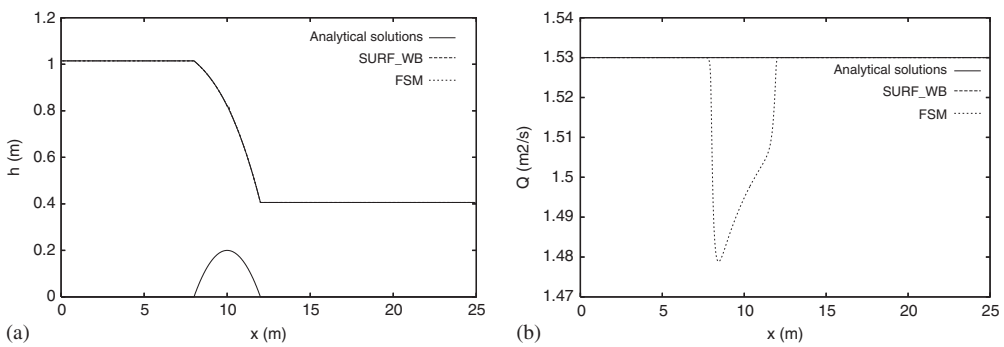

Figure A1. Transcritical flow without shock over a bump. Comparison between *SURF_WB*, classical FSM and analytical solutions for: (a) the water depth h; and (b) the discharge $Q = (hu)$ at $t = 200\,\text{s}$.

DOI: 10.1002/fld

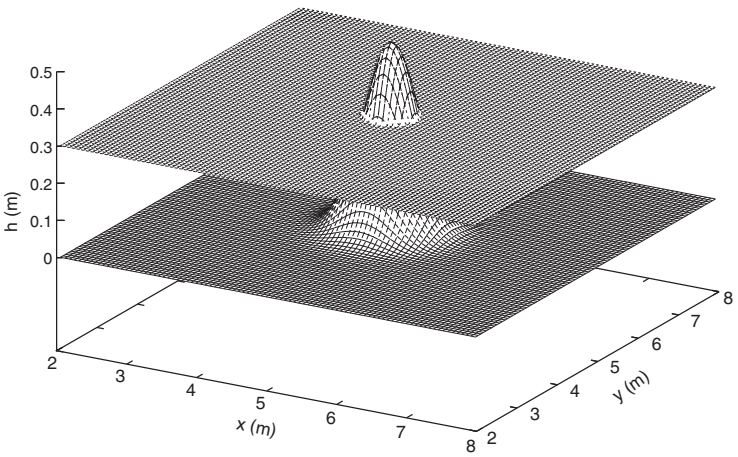

Figure A2. 2D flow at rest. Initial condition.

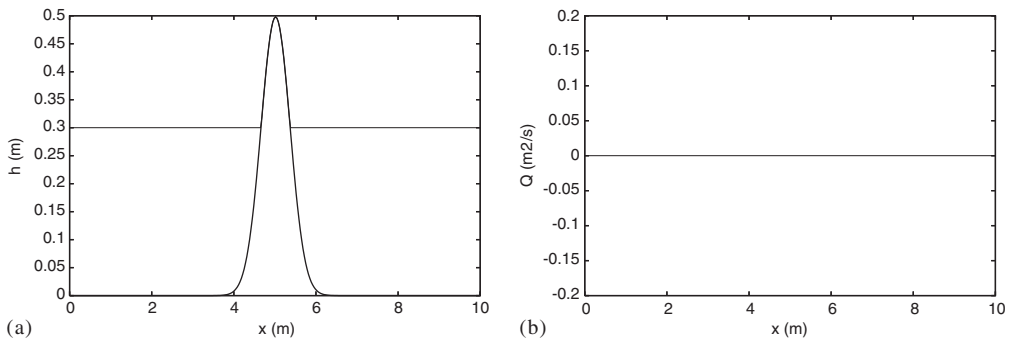

Figure A3. 2D flow at rest. Centreline profiles of: (a) the surface elevation; and (b) the discharge, at $t = 400\,\mathrm{s}$.

homogeneous system) are similar and very close to the analytical solution. This situation is not true for the discharge and we can observe in Figure A1(b) the real improvement brought up by the well-balanced approach since the discharge Q computed by *SURF_WB* is almost constant, whereas the FSM induces non-physical oscillations over topography variations.

A.2. A two-dimensional flow at rest with a dry area

The initial condition of this test is a two-dimensional flow at rest. This test aims at showing that the 'second order' accuracy well-balanced approach used in *SURF_WB* is able to preserve a steady state 'at rest', as expected from the hydrostatic reconstruction, and that the two-dimensional extension on Cartesian meshes does not modify this property. We impose $h + d = \max(d, 0.3)\,\mathrm{m}$ and $Q = 0\,\mathrm{m}^2/\mathrm{s}$ over the whole domain, which contains 150×150 cells. The topography is defined

DOI: 10.1002/fld

as follows:

$$d(x, y) = 0.5 \exp(-(r/\sigma)^2) \tag{A1}$$

where $r = \sqrt{x^2 + y^2}$, $\sigma = 0.5$ and $(x_0, y_0) = (5, 5)$. The initial condition at rest is plotted in Figure A2. We can observe in Figures A3(a) and (b) the results obtained at $t = 400$ s for the centerline profiles at $y = 0$ of surface elevation and discharge. As expected, the *SURF_WB* model exactly preserves the steady state. Though it is not shown here, the results remains reliable even when the initial conditions are $h + d = \max(d, 0.6)$ m (no dry cells) or $h = 0$ m (no water).

ACKNOWLEDGEMENTS

The authors wish to thank E. Audusse, T. Gallouët and A. Y. Leroux for fruitful discussions.

REFERENCES

1. de Saint Venant AJC. Théorie du mouvement non-permanent des eaux, avec application aux crues des rivières et à l'introduction des marèes dans leur lit. *Comptes Rendus de l' Academie des Sciences*, *Paris* 1871; **73**:147–154.
2. Hibberd S, Peregrine DH. Surf and run-up on a beach: a uniform bore. *Journal of Fluid Mechanics* 1979; **95**(2):323–345.
3. Kobayashi N, Otta AK, Roy I. Wave reflection and run-up on rough slopes. *Journal of Waterway Port Coastal and Ocean Engineering* 1987; **113**(3):282–298.
4. Casulli V. A semi-implicit finite difference method for non-hydrostatic free-surface flows. *International Journal for Numerical Methods in Fluids* 1999; **30**:425–440.
5. Van't Hof B, Vollebregt EAH. Modelling of wetting and drying of shallow water using artificial porosity. *International Journal for Numerical Methods in Fluids* 2005; **48**:1199–1217.
6. Stelling GS, Duinmeijer SPA. A staggered conservative scheme for every Froude number in rapidly shallow water flows. *International Journal for Numerical Methods in Fluids* 2003; **43**:1329–1354.
7. Zelt JA. Tsunamis: the response of harbors with sloping boundaries to long wave excitation. *Technical Report KH-R-47*, California Institute of Technology, 1986.
8. Özkan-Haller HT, Kirby JT. A Fourier–Chebyshev collocation method for the shallow water equations including shoreline runup. *Applied Ocean Research* 1997; **19**:21–34.
9. Brocchini M, Svendsen IA, Prasad RS, Belloti G. A comparison of two different types of shoreline boundary conditions. *Computer Methods in Applied Mechanics and Engineering* 2002; **191**:4475–4496.
10. Hu K, Mingham CG, Causon DM. Numerical simulation of wave overtopping of coastal structures using the non-linear shallow water equations. *Coastal Engineering* 2000; **41**:433–465.
11. Brocchini M, Bernetti R, Mancinelli A, Albertini G. An efficient solver for nearshore flows based on the WAF method. *Coastal Engineering* 2001; **43**:105–129.
12. Toro EF. The weighted average flux method applied to the time-dependent Euler equation. *Philosophical Transactions of the Royal Society of London Series A—Mathematical Physical and Engineering Sciences* 1992; **341**:499–530.
13. Hubbard ME, Dodd N. A 2D numerical model of wave run-up and overtopping. *Coastal Engineering* 2002; **47**:1–26.
14. Yanenko NN. *Méthodes à pas fractionnaires. Résolution de problèmes polydimensionels de physique mathématique*. Armand Colin, 1968.
15. Greenberg JM, Leroux AY. A well balanced scheme for the numerical processing of source terms in hyperbolic equations. *SIAM Journal on Numerical Analysis* 1996; **33**(1):1–16.
16. Leveque RJ. Balancing source terms and flux gradients in high resolution Godunov methods: the quasi-steady wave-propagation algorithm. *Journal of Computational Physics* 1998; **146**:346–365.
17. Bermudez A, Vazquez-Cendon ME. Upwind methods for hyperbolic conservation laws with source terms. *Computers and Fluids* 1994; **23**:1049–1071.

DOI: 10.1002/fld

18. Bermudez A, Dervieux A, Desideri JA, Vasquez ME. Upwind schemes for two-dimensional shallow water equations with variable depth using unstructured meshes. *Computer Methods in Applied Mechanics and Engineering* 1998; **155**:49–72.
19. Zhou JG, Causon DM, Mingham CG, Ingram DM. The surface gradient method for the treatment of source terms in the shallow-water equations. *Journal of Computational Physics* 2001; **168**:1–25.
20. Gosse L. A well balanced flux-vector splitting scheme designed for the hyperbolic systems of conservation laws with source terms. *Computers and Mathematics with Applications* 2000; **39**(1):135–159.
21. Gallouët T, Herard JM, Seguin N. Some approximate Godunov schemes to compute shallow-water equations with topography. *Computers and Fluids* 2003; **32**:479–513.
22. Chinnayya A, Leroux AY, Seguin N. A well-balanced numerical scheme for the approximation of the shallow-water equations with topography: the resonance phenomenon. *International Journal on Finite Volumes* 2004.
23. Audusse E, Bouchut F, Bristeau MO, Klein R, Perthame B. A fast and stable well-balanced scheme with hydrostatic reconstruction for shallow water flows. *SIAM Journal on Scientific Computing* 2004; **25**(6):2050–2065.
24. Gallouët T, Herard JM, Seguin N. On the use of some symmetrizing variables to deal with vacuum. *Calcolo* 2003; **40**:163–194.
25. Eymard R, Gallouët T, Herbin R. Finite volume methods. In *Handbook of Numerical Analysis*, Ciarlet PG, Lions JL (eds), vol. III. North-Holland: Amsterdam, 2000; 729–1020.
26. Carrier GF, Greenspan HP. Water waves of finite amplitude on a sloping beach. *Journal of Fluid Mechanics* 1958; **4**:97–109.
27. Van Leer B. Towards the ultimate conservative difference scheme V. A second order sequel to Godunov's method. *Journal of Computational Physics* 1979; **32**:101–136.
28. Kobayashi N, Desilva GS, Watson KD. Wave transformation and swash oscillation on gentle and steep slopes. *Journal of Geophysical Research* 1989; **94**:951–966.
29. Lynett PJ, Wu TR, Liu PL-F. Modeling wave run-up with depth-integrated equations. *Coastal Engineering* 2002; **46**:89–107.
30. Synolakis CE. The runup of solitary waves. *Journal of Fluid Mechanics* 1987; **185**:523–545.
31. Thacker WC. Some exact solutions to the nonlinear shallow-water wave equations. *Journal of Fluid Mechanics* 1981; **107**:499–508.
32. Marche F, Bonneton P. A simple and efficient well-balanced scheme for 2D bore propagation and run-up over a sloping beach. *Proceedings of the International Conference on Coastal Engineering ICCE*, 2006, in press.
33. Brocchini M, Bernetti R, Mancinelli A, Soldini L. Structure-generated macrovortices and their evolution in very shallow depths. *Proceedings of the 28th International Conference on Coastal Engineering*, vol. 1. ASCE, 2002; 772–783.
34. Goutal N, Maurel F. *Proceedings of the 2nd Workshop on Dam-Break Wave Simulation*, *EDF-DER Report HE-43/97/016/B*, 1997.

DOI: 10.1002/fld